Intensity of Waves Inside a Strongly Disordered Medium

S. E. Skipetrov*
Univ. Grenoble Alpes, CNRS, LPMMC, 38000 Grenoble, France

I. M. Sokolov†
Department of Theoretical Physics, Peter the Great St. Petersburg Polytechnic University, 195251 St. Petersburg, Russia

(Received 10 July 2019; published 4 December 2019)

Anderson localization does not lead to an exponential decay of intensity of an incident wave with the depth inside a strongly disordered three-dimensional medium. Instead, the average intensity is roughly constant in the first half of a disordered slab, sharply drops in a narrow region in the middle of the sample, and then remains low in the second half of the sample. A universal, scale-free spatial distribution of average intensity is found at mobility edges where the intensity exhibits strong sample-to-sample fluctuations. Our numerical simulations allow us to discriminate between two competing local diffusion theories of Anderson localization and to pinpoint a deficiency of the self-consistent theory.

DOI: 10.1103/PhysRevLett.123.233903

Studies of wave propagation in disordered media mainly focus on the scattering problem in which one is interested in determining a relation between incident and scattered waves outside the disordered sample and often even in the far field of it [1,2]. Transmission and reflection coefficients of disordered media have been extensively studied in this context, including their statistics and correlations [2]. Scattered waves outside the medium are not only easier to measure, they are also relevant for understanding practically important quantities, such as the electrical conductance of metals [3] or the whiteness of paints [4], as well as for developing applications for complex material [5] or biological tissue [6] sensing, imaging through opaque, turbid media [7], or cryptography [8]. In contrast, the spatial distribution of wave intensity *inside* a disordered medium has attracted much less attention even though it is important for such prospective applications of disordered materials as light harvesting in solar cells [9], random lasing [10], optical frequency conversion [11], or photoacoustic tomography [12]. For three-dimensional (3D) media we know that the average intensity exhibits diffusive behavior for weak disorder and hence, in the absence of absorption, decays linearly with the depth inside a disordered layer (slab) illuminated by a plane wave [1,2]. However, nothing is known at the moment about the way in which this linear behavior is modified when the disorder becomes strong enough for reaching a critical point of the Anderson localization transition (a mobility edge) and crossing it to enter the Anderson localization regime [13,14].

The spatial distribution of the average wave intensity $\langle I(\mathbf{r})\rangle$ inside a strongly disordered medium of length L illuminated by a monochromatic wave has been studied theoretically for a one-dimensional (1D) medium [15–18] and for a quasi-one dimensional (quasi-1D) waveguide [19–21]. In both cases, the behavior of $\langle I(\mathbf{r})\rangle = \langle I(z)\rangle$ differs from a simple exponential decay with the distance z from the sample boundary. This suggests that the exponential decay of eigenmodes in space does not directly map to the exponential decay of the average intensity. Instead, $\langle I(z)\rangle$ exhibits a steplike shape, first remaining virtually constant with z, then dropping sharply in a narrow region around the middle of the disordered sample $z = L/2$, and finally remaining low for $L/2 < z < L$. A tendency towards such a behavior has been experimentally observed by Yamilov *et al.* in two-dimensional (2D) quasi-1D waveguides [22].

In this Letter we use *ab initio* numerical simulations of wave scattering in large 3D ensembles of point scatterers and the local diffusion theories of Anderson localization to discover two important results. First, we show that the behavior that was previously found for $\langle I(z)\rangle$ in 1D and quasi-1D samples, generalizes to 3D slabs, provided that the disorder is strong enough for reaching Anderson localization. Two competing local diffusion theories—the self-consistent (SC) theory of Anderson localization and the supersymmetric (SUSY) field theory—yield analytic expressions for $\langle I(z)\rangle$ as a function of z/L that are parametrized by a single parameter L/ξ, where L is the slab thickness and ξ is the localization length. Second, we compute $\langle I(z)\rangle$ at a mobility edge, i.e., in the critical regime that does not exist in low-dimensional systems. Analytic expressions for $\langle I(z)\rangle$ following from SC and SUSY theories become scale independent for L much exceeding the mean free path ℓ. By repeating calculations for light scattering by atoms in a strong magnetic field we

demonstrate that our results are universal and hold beyond the scalar wave model. This completes the palette of behaviors expected for $\langle I(z)\rangle$ for any disorder strength, any dimensionality of space, and for both scalar and vector waves. Comparison of SC theory with numerical simulations and SUSY theory confirms its validity at the mobility edge but reveals its deficiency in the Anderson localization regime. Understanding limitations of SC theory is important in view of its applications for interpretation of 3D acoustic [23,24] and cold-atom [25] experiments as well as of large-scale numerical simulations of light localization [26].

We consider a monochromatic plane wave $\psi_0(\mathbf{r}) = \exp(ikz)$ incident at $z = 0$ on a disordered sample (slab) confined between the planes $z = 0$ and $z = L$ and having a shape of a cylinder of length (thickness) L, radius $R \gg L$ and volume $V = \pi R^2 L$. We denote the frequency of the wave by ω and its wave number by $k = \omega/c$, where c is the speed of the wave in the homogeneous medium by which the sample is surrounded. Our point-scatterer model assumes that the sample is simply an ensemble of $N \gg 1$ identical resonant point scatterers with a polarizability $\alpha(\omega) = -(\Gamma_0/2)/(\omega - \omega_0 + i\Gamma_0/2)$ located at random positions $\{\mathbf{r}_m\}$, $m = 1, \ldots, N$, inside the slab. The resonance width Γ_0 is assumed to be much smaller than the resonance frequency ω_0 of an individual scatterer. A vector $\boldsymbol{\psi} = [\psi(\mathbf{r}_1), \ldots, \psi(\mathbf{r}_N)]^T$ of wave amplitudes at scatterer positions obeys [27,28]

$$\boldsymbol{\psi} = \boldsymbol{\psi}_0 + \alpha(\omega)[\hat{G}(\omega) - i\mathbb{1}]\boldsymbol{\psi}, \tag{1}$$

where $\boldsymbol{\psi}_0 = [\psi_0(\mathbf{r}_1), \ldots, \psi_0(\mathbf{r}_N)]^T$ and

$$G_{mn}(\omega) = i\delta_{mn} + (1 - \delta_{mn})\frac{\exp(ik|\mathbf{r}_m - \mathbf{r}_n|)}{k|\mathbf{r}_m - \mathbf{r}_n|}. \tag{2}$$

The solution of Eq. (1) reads

$$\boldsymbol{\psi} = (\mathbb{1} - \alpha(\omega)[\hat{G}(\omega) - i\mathbb{1}])^{-1}\boldsymbol{\psi}_0. \tag{3}$$

We compute the average intensity $\langle I(\mathbf{r})\rangle$ inside the sample by averaging $|\psi(\mathbf{r}_m)|^2$ over all $\mathbf{r}_m$ inside a small volume around $\mathbf{r}$ and over many (up to 5×10^5) random and statistically independent scatterer configurations $\{\mathbf{r}_m\}$. In addition, $\langle I(\mathbf{r})\rangle$ is averaged over a sufficiently large circular area of radius R_1 around the sample axis ($1/k \ll R_1 < R$) in order to obtain $\langle I(z)\rangle$ which is independent of $\mathbf{r}_\perp = \{x, y\}$ and mimics the average intensity in a disordered slab of infinite transverse extent $R \to \infty$.

We have extensively studied Anderson localization in the model defined by Eqs. (1)–(3) in our previous works [29,30]. In particular, we have found that spatially localized modes appear in a narrow frequency band between two density-dependent mobility edges $\omega_c^{\mathrm{I}} = \omega_c^{\mathrm{I}}(\rho/k_0^3)$ and $\omega_c^{\mathrm{II}} = \omega_c^{\mathrm{II}}(\rho/k_0^3)$ for scatterer number densities $\rho = N/V$ exceeding a critical value $\rho_c \simeq k_0^3/4\pi$, where $k_0 = \omega_0/c$. We will use these previous results to study $\langle I(z)\rangle$ in the localized regime by choosing the frequency $\omega \in (\omega_c^{\mathrm{I}}, \omega_c^{\mathrm{II}})$ and in the critical regime for $\omega = \omega_c^{\mathrm{I}}$ or $\omega = \omega_c^{\mathrm{II}}$.

The results of the point-scatterer model (1)–(3) will be compared to two competing local diffusion theories of Anderson localization [31–35]. In these theories, the average intensity of a wave $\langle I(\mathbf{r})\rangle$ obeys a diffusion equation with a position-dependent diffusivity $D(\mathbf{r})$:

$$-\boldsymbol{\nabla} \cdot D(\mathbf{r})\boldsymbol{\nabla}\langle I(\mathbf{r})\rangle = S(\mathbf{r}), \tag{4}$$

where $S(\mathbf{r})$ describes the distribution of wave sources in the medium. In three dimensions, the position dependence of $D(\mathbf{r})$ in Eq. (4) arises only for strong disorder and can be found in two different ways. First, SC theory of localization [31,36,37] yields $D(\mathbf{r})$ determined self-consistently via the return probability $P(\mathbf{r}, \mathbf{r}' = \mathbf{r})$ found as a solution of Eq. (4) with $S(\mathbf{r}) = \delta(\mathbf{r} - \mathbf{r}')$ and an appropriate cutoff procedure to regularize the unphysical divergence of the solution for $\mathbf{r}' = \mathbf{r}$ [31,32]:

$$\frac{1}{D(\mathbf{r})} = \frac{1}{D_B} + \frac{12\pi}{K^2\ell} P(\mathbf{r}, \mathbf{r}), \tag{5}$$

where D_B is the bare value of D in the absence of localization effects and K is the effective wave number in the disordered medium. In a slab, Eqs. (4) and (5) should be solved with appropriate boundary conditions for $P(\mathbf{r}, \mathbf{r}')$ [38]. A second approach is based on field-theoretic, SUSY methods and has been mainly developed for 1D and quasi-1D media [33–35]. It does not provide a simple microscopic expression or an equation for $D(\mathbf{r})$ that would hold for any sample geometry, but it yields a scaling relation between $D_\infty(z)$ in the semi-infinite medium and $D(z)$ in a slab of finite thickness L [34].

Interestingly enough, both SC and SUSY theories yield $D_\infty(z) = D(0)\exp(-2z/\xi)$ in the Anderson localization regime ($K\ell < 1$) [44], but solutions for the slab geometry differ. SC theory yields a result that for $L \gg \xi$ is well described by an interpolation formula $D_{\mathrm{SC}}(z) = [D_\infty(z)^{1/2} + D_\infty(L - z)^{1/2}]^2$ [38]. The SUSY approach yields a different result: $D_{\mathrm{SUSY}}(z) = D_\infty[z(L - z)/L]$ [34]. In both cases, flux conservation implies that the diffusive flux J_{dif} given by the Fick's law $J_{\mathrm{dif}} = -D(z)\partial\langle I(z)\rangle/\partial z$ is independent of z for $z \gg \ell$. Integrating the Fick's law yields

$$\langle I(z)\rangle = I_0 - J_{\mathrm{dif}} \int_0^z \frac{dz'}{D(z')} \quad \text{for } z \gg \ell, \tag{6}$$

where the precise value of I_0 depends on the details of conversion of the incident plane wave into diffuse radiation near the sample surface $z = 0$. Supplemented with a boundary condition $\langle I(L)\rangle = 0$ [2], Eq. (6) yields

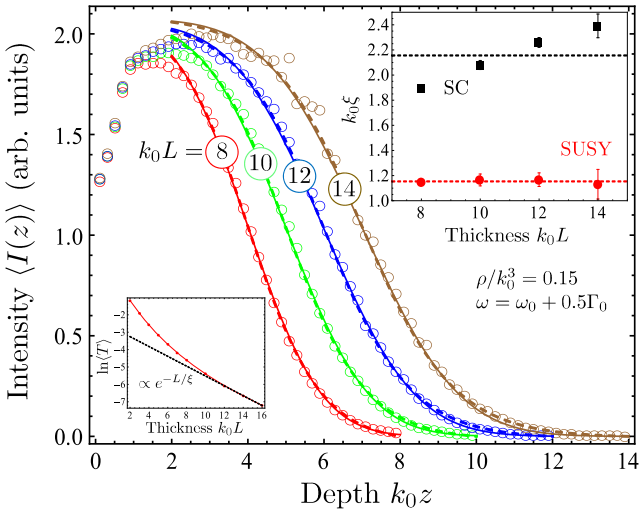

FIG. 1. Spatial distributions of the average wave intensity inside slabs of disordered medium of different thicknesses $k_0 L = 8$–14. Symbols correspond to the point-scatterer model (1) with ω in between the two mobility edges $\omega_c^{\mathrm{I}} = \omega_0 + 0.256\Gamma_0$ and $\omega_c^{\mathrm{II}} = \omega_0 + 0.935\Gamma_0$ for $\rho/k_0^3 = 0.15$ [30], $k_0 R = 20$, and $k_0 R_1 = 10$. Almost coinciding dashed and solid lines show fits of SC (7) and SUSY (8) theories to the point-scatterer data for $k_0 z > 2$ with the localization length ξ as a free parameter. The upper inset shows the best-fit values of ξ following from SC (black squares) and SUSY (red circles) theories. Dashed lines show average values of ξ. The lower inset shows the average transmission through the slab as a function of slab thickness.

$$\langle I(z)\rangle_{\mathrm{SC}} = I_0 \frac{\sinh[(L-z)/\xi]}{\sinh(z/\xi) + \sinh[(L-z)/\xi]}, \tag{7}$$

$$\langle I(z)\rangle_{\mathrm{SUSY}} = \frac{I_0}{2}\left(1 + \frac{\mathrm{erf}[(L-2z)/\sqrt{2L\xi}]}{\mathrm{erf}(\sqrt{L/2\xi})}\right), \tag{8}$$

where $\mathrm{erf}(x)$ is the error function.

The point-scatterer model and SC and SUSY theories yield consistent results for the distribution of the average intensity $\langle I(z)\rangle$ inside the disordered slab in the localized regime. As we see from Fig. 1, $\langle I(z)\rangle$ does not decay exponentially with z as one could expect from naive considerations, but instead exhibits a rapid drop near the middle of the slab, while varying much slower near its boundaries. Such a behavior is similar to that found previously in 1D [15–19] and quasi-1D [20,21] media.

Even though both SC and SUSY theories provide good and, in fact, hardly distinguishable fits to the numerical data, only the SUSY model consistently yields the same (within error bars) best-fit values of ξ for different L as we show in the inset of Fig. 1. The underlying problem of the SC model is best demonstrated by computing the width δ of the spatial region in which the average intensity changes rapidly near the middle of the sample:

$$\delta = \left[-\frac{1}{\langle I(z)\rangle}\frac{\partial}{\partial z}\langle I(z)\rangle\right]^{-1}\Bigg|_{z=L/2}. \tag{9}$$

We find $\delta_{\mathrm{SC}} = \xi$ and $\delta_{\mathrm{SUSY}} = \sqrt{(\pi/8)L\xi}$ for $L \gg \xi$, which predict different scalings of δ with L. The need for different values of ξ to fit the numerical data corresponding to different L with SC theory signals that the scaling that it predicts for δ is wrong. In contrast, SUSY theory yields the correct scaling for δ and describes the data in Fig. 1 with a single value of ξ for all L.

An interesting regime that is not accessible in low-dimensional systems is the critical one. In order to study it in the framework of the point-scatterer model (1), we choose the frequency of the wave ω exactly at one of the mobility edges $\omega_c^{\mathrm{I,II}}$ determined in Ref. [30]. The resulting spatial distributions of $\langle I(z)\rangle$ are shown in Fig. 2 by symbols. To study the critical regime using the local diffusion theories, we note that for a semi-infinite medium ($L \to \infty$) one finds $D(z) = D_\infty(z) \simeq D(0)/(1 + z/\eta)$ [31] with a decay length $\eta \sim \ell$. For a slab of finite thickness L, the results of SC theory may be nicely interpolated by $D(z) = [D_\infty(z)^2 + D_\infty(L-z)^2]^{1/2}$ [38], whereas another option is to extrapolate the relation $D_{\mathrm{SUSY}}(z) = D_\infty[z(L-z)/L]$ [34,35] to the mobility edge. Proceeding in the same way as for deriving Eqs. (7) and (8), we obtain expressions for $\langle I(z)\rangle$ that depend on z/L and L/η. The full expression following from SC theory is quite cumbersome and we reproduce it elsewhere [38] whereas the SUSY result is simpler:

$$\langle I(z)\rangle_{\mathrm{SUSY}} = I_0\left(1 - \frac{z}{L}\right)\left[1 + \frac{\frac{z}{L}(1 - 2\frac{z}{L})}{1 + 6\frac{\eta}{L}}\right]. \tag{10}$$

Comparison of these results with numerical simulations of the model (1) is shown in Fig. 2. The agreement is less striking than in the localized regime but it improves when L increases. In addition, variations of the best-fit η with L are similar for SC and SUSY theories but differ from SC theory expectations [38]. Universal, parameter-free intensity distributions follow in the limit of $L \gg \eta$:

$$\langle I(z)\rangle_{\mathrm{SC}} = \frac{I_0}{2}\left\{1 + \frac{3\sqrt{2}\,\mathrm{arcsinh}(1-2\frac{z}{L}) - 2(1-2\frac{z}{L})\sqrt{1-2\frac{z}{L}(1-\frac{z}{L})}}{3\sqrt{2}\,\mathrm{arcsinh}(1) - 2}\right\}, \tag{11}$$

$$\langle I(z)\rangle_{\mathrm{SUSY}} = I_0\left(1 - \frac{z}{L}\right)^2\left(1 + 2\frac{z}{L}\right). \tag{12}$$

These two expressions are very close when plotted as functions of z/L. Their lack of any characteristic length scale can be seen as a consequence of the fractal character of critical eigenmodes [45]. By analogy with other models

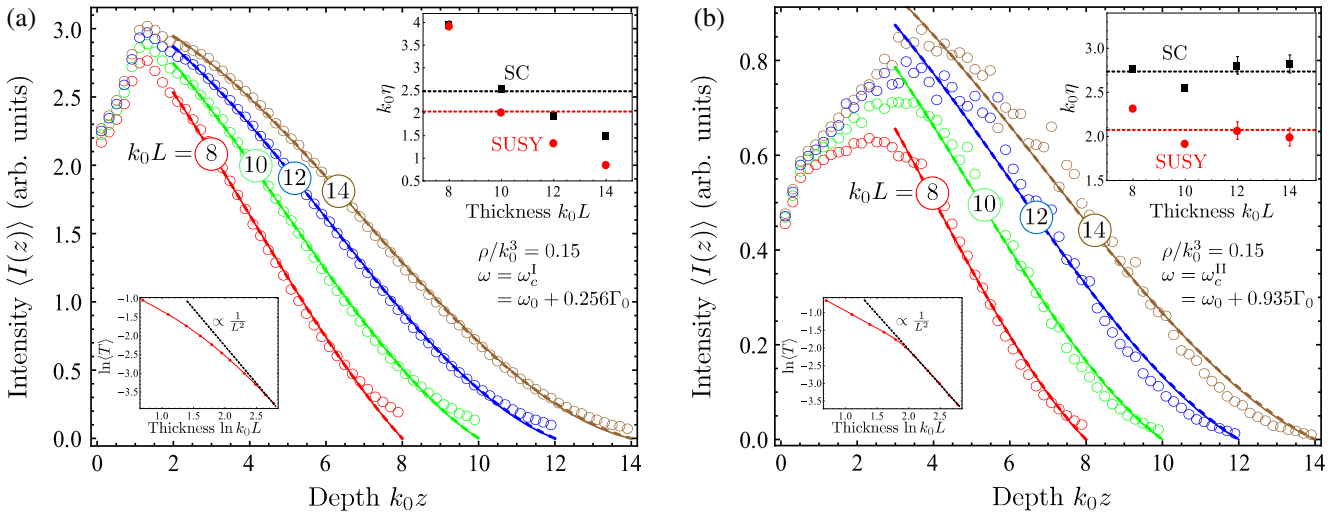

FIG. 2. Same as Fig. 1 but at the low- (a) and high-frequency (b) mobility edges $\omega = \omega_c^{\rm I}$ and $\omega = \omega_c^{\rm II}$, respectively, and for $k_0 R = 25$. Dashed and solid lines show, respectively, SC and SUSY theory fits to numerical results with the decay length η as a free fit parameter. The fits were performed for $k_0 z > 2$ (a) or $k_0 z > 3$ (b). The upper insets show the best-fit values of η for SC (black squares) and SUSY (red circles) models, with average values of η represented by dashed lines. The lower insets show the average transmission through the slab as a function of slab thickness.

of Anderson localization [45,46], we expect the critical eigenmodes of our model defined by Eqs. (1)–(3) to be *multifractal*, but evidencing this would require analysis of higher-order statistical moments and spatial correlations of intensity in addition to the study of its average value.

Comparison of results corresponding to the two mobility edges $\omega = \omega_c^{\rm I}$ and $\omega = \omega_c^{\rm II}$ suggests that the behaviors of our point-scatterer model at these frequencies are quite different. First, the mean free path ℓ can be estimated as a position of the maximum of $\langle I(z)\rangle$ in Figs. 2(a) or 2(b) and turns out to be considerably larger at the second, high-frequency mobility edge. As a consequence, the results presented in Fig. 2(b) correspond to shorter optical thicknesses L/ℓ than the data in Fig. 2(a). Second, the sample-to-sample fluctuations of intensity at the second mobility edge are much stronger than at the first one. This is illustrated in Fig. 3(a) where we show the relative intensity fluctuation $\sigma = \sqrt{\langle \delta I(\mathbf{r})^2\rangle}/\langle I(z)\rangle$, where $\delta I(\mathbf{r}) = I(\mathbf{r}) - \langle I(z)\rangle$, as a function of z for $k_0 L = 12$. We attribute this difference to subradiant states localized on pairs of closely located scatterers and surviving multiple scattering only for small interatomic distances and hence large frequency shifts $(\omega - \omega_0)/\Gamma_0$ [29]. Figure 3(b) shows the inverse participation ratio $\mathrm{IPR}_n = \sum_m |\psi_n(\mathbf{r}_m)|^4$ of eigenvectors $\boldsymbol{\psi}_n$ of the matrix $\hat{G}(\omega_0)$ (quasimodes) as a function of their frequencies ω and decay rates Γ. Note that whereas the low-frequency mobility edge I defines a sharp transition between extended states for $\omega < \omega_c^{\rm I}$ (low IPR, light gray points) and localized states for $\omega_c^{\rm I} < \omega < \omega_c^{\rm II}$ (high IPR, dark gray and black points), there are localized states on both sides from the mobility edge II. However, the physical origin of quasimode localization is different for $\omega_c^{\rm I} < \omega < \omega_c^{\rm II}$ (localization due to strong scattering appearing only for $N \gg 1$ and $\rho > \rho_c$) and $\omega > \omega_c^{\rm II}$ (localization that exists for any $N \geq 2$ and any ρ). This difference is manifest in the scaling properties of quasimode properties with sample size [29]. Its link with existence of two-atom subradiant states is further confirmed by a more detailed analysis [38].

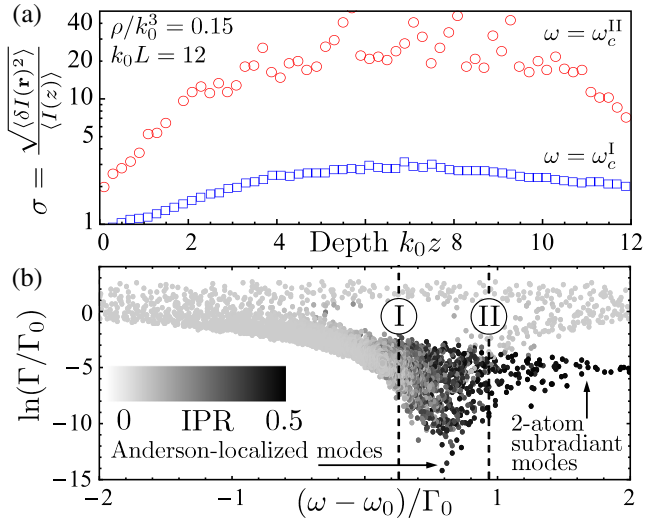

FIG. 3. (a) Relative fluctuations of intensity at the two mobility edges for a slab of thickness $k_0 L = 12$ and all other parameters as in Fig. 2. (b) Gray scale plot of IPR of quasimodes for a representative random configuration of scatterers. Each point corresponds to a quasimode of frequency $\omega = \omega_0 - (\Gamma_0/2)\mathrm{Re}\Lambda$ and decay rate $\Gamma = \Gamma_0 \mathrm{Im}\Lambda$, where Λ is an eigenvalue of $\hat{G}(\omega_0)$. The gray scale of the point reflects the IPR of the corresponding eigenvector. Dashed lines show the two mobility edges.

In conclusion, we have found analytic formulas for the spatial distribution of average wave intensity $\langle I(z)\rangle$ inside a thick 3D slab of strongly disordered medium illuminated by a monochromatic plane wave. In the Anderson localization regime, $\langle I(z)\rangle$ exhibits a steplike shape and drops sharply within a region of width $\delta \sim \sqrt{L\xi}$ in the middle of the sample. At a mobility edge, $\langle I(z)\rangle$ takes a universal, parameter-free shape as a function of z/L. Comparison of *ab initio* numerical simulations with local diffusion theories allowed us to reveal a deficiency of SC theory for a description of Anderson localization in three dimensions. A realistic physical system in which Anderson localization of light can be observed is a large ensemble of cold atoms in a strong magnetic field [47,48]. Repeating all the calculations presented above for this system yields very similar results [38]. In a cloud of two-level cold atoms, intensity of light is proportional to the population of the excited state and therefore its spatial distribution can be imaged by the so-called diffraction-contrast imaging [49], allowing for state-selective imaging of atoms [50] by monitoring a slow spontaneous decay of the excited state to a third, auxiliary level, or by probing the excited level by a weak probe beam resonant with a transition to a higher-energy state. In a dielectric disordered system, spatial distribution of optical intensity can be imaged by opto-acoustic methods [51].

Numerical calculations of the spatial distributions of average intensity and of the transmission coefficients were carried out with the financial support of the Russian Science Foundation (Project No. 17-12-01085). I. M. S. acknowledges the hospitality of the LPMMC where a part of this work has been performed with the financial support of the Centre de Physique Théorique de Grenoble-Alpes (CPTGA).

*Sergey.Skipetrov@lpmmc.cnrs.fr
†ims@is12093.spb.edu

[1] P. Sheng, *Introduction to Wave Scattering, Localization, and Mesoscopic Phenomena* (Springer, Heidelberg, 2006).
[2] E. Akkermans and G. Montambaux, *Mesoscopic Physics of Electrons and Photons* (Cambridge University Press, Cambridge, England, 2007).
[3] J. S. Dugdale, *The Electrical Properties of Disordered Metals* (Cambridge University Press, Cambridge, England, 1995).
[4] B. R. Palmer, P. Stamatakis, C. F. Bohren, and G. C. Salzman, A multiple-scattering model for opacifying particles in polymer-films, J. Coat. Technol. **61**, 41 (1989).
[5] F. Scheffold and P. Schurtenberger, Light scattering probes of viscoelastic fluids and solids, Soft Mater. **1**, 139 (2003).
[6] T. Durduran, R. Choe, W. B. Baker, and A. G. Yodh, Diffuse optics for tissue monitoring and tomography, Rep. Prog. Phys. **73**, 076701 (2010).
[7] O. Katz, P. Heidmann, M. Fink, and S. Gigan, Non-invasive single-shot imaging through scattering layers and around corners via speckle correlations, Nat. Photonics **8**, 784 (2014).
[8] S. A. Goorden, M. Horstmann, A. P. Mosk, B. Škoric, and P. W. H. Pinkse, Quantum-secure authentication of a physical unclonable key, Optica **1**, 421 (2014).
[9] K. Vynck, M. Burresi, F. Riboli, and D. S. Wiersma, Photon management in two-dimensional disordered media, Nat. Mater. **11**, 1017 (2012).
[10] D. S. Wiersma, The physics and applications of random lasers, Nat. Phys. **4**, 359 (2008).
[11] R. Fischer, S. M. Saltiel, D. N. Neshev, W. Krolikowski, and Y. S. Kivshar, Broadband femtosecond frequency doubling in random media, Appl. Phys. Lett. **89**, 191105 (2006).
[12] L. V. Wang and S. Hu, Photoacoustic tomography: In vivo imaging from organelles to organs, Science **335**, 1458 (2012).
[13] P. W. Anderson, Absence of diffusion in certain random lattices, Phys. Rev. **109**, 1492 (1958).
[14] A. Lagendijk, B. A. van Tiggelen, and D. S. Wiersma, Fifty years of Anderson localization, Phys. Today **62**, No. 8, 24 (2009).
[15] Yu. L. Gazaryan, The one-dimensional problem of propagation of waves in a medium with random inhomogeneities, Sov. Phys. JETP **29**, 996 (1969).
[16] P. Lang, Probability density function and moments of the field in a slab of one-dimensional random medium, J. Math. Phys. (N.Y.) **14**, 1921 (1973).
[17] B. S. Abramovich, S. N. Gurbatov, and Yu. A. Ryzhov, Multiple scattering in a one-dimensional, randomly non-uniform medium, Radiophys. Quantum Electron. **22**, 389 (1979).
[18] P. A. Mello, Z. Shi, and A. Z. Genack, Connection between wave transport through disordered 1D waveguides and energy densityinside the sample: A maximum-entropy approach, Physica (Amsterdam) **82E**, 261 (2016).
[19] L.-Y. Zhao, C.-S. Tian, Z.-Q. Zhang, and X.-D. Zhang, Unconventional diffusion of light in strongly localized open absorbing media, Phys. Rev. B **88**, 155104 (2013).
[20] B. A. van Tiggelen, S. E. Skipetrov, and J. H. Page, Position-dependent radiative transfer as a tool for studying Anderson localization: Delay time, time-reversal and coherent backscattering, Eur. Phys. J. Spec. Top. **226**, 1457 (2017).
[21] X. Cheng, C. Tian, Z. Lowell, L. Zhao, and A. Z. Genack, Impact of surface reflection on transmission eigenvalue statistics and energy distributions inside random media, Eur. Phys. J. Spec. Top. **226**, 1539 (2017).
[22] A. G. Yamilov, R. Sarma, B. Redding, B. Payne, H. Noh, and H. Cao, Position-Dependent Diffusion of Light in Disordered Waveguides, Phys. Rev. Lett. **112**, 023904 (2014).
[23] L. A. Cobus, S. E. Skipetrov, A. Aubry, B. A. van Tiggelen, A. Derode, and J. H. Page, Anderson Mobility Gap Probed by Dynamic Coherent Backscattering, Phys. Rev. Lett. **116**, 193901 (2016).
[24] L. A. Cobus, W. K. Hildebrand, S. E. Skipetrov, B. A. van Tiggelen, and J. H. Page, Transverse confinement of ultrasound through the Anderson transition in three-dimensional mesoglasses, Phys. Rev. B **98**, 214201 (2018).
[25] F. Jendrzejewski, A. Bernard, K. Müller, P. Cheinet, V. Josse, M. Piraud, L. Pezzé, L. Sanchez-Palencia, A. Aspect,

and P. Bouyer, Three-dimensional localization of ultracold atoms in an optical disordered potential, Nat. Phys. **8**, 398 (2012).

[26] J. Haberko, L. S. Froufe-Pérez, and F. Scheffold, Transition from light diffusion to localization in three-dimensional hyperuniform dielectric networks near the band edge, arXiv:1812.02095.

[27] L. L. Foldy, The multiple scattering of waves: I. General theory of isotropic scattering by randomly distributed scatterers, Phys. Rev. **67**, 107 (1945).

[28] M. Lax, Multiple scattering of waves, Rev. Mod. Phys. **23**, 287 (1951).

[29] S. E. Skipetrov, Finite-size scaling analysis of localization transition for scalar waves in a three-dimensional ensemble of resonant point scatterers, Phys. Rev. B **94**, 064202 (2016).

[30] S. E. Skipetrov and I. M. Sokolov, Ioffe-Regel criterion of Anderson localization in the model of resonant point scatterers, Phys. Rev. B **98**, 064207 (2018).

[31] B. A. van Tiggelen, A. Lagendijk, and D. S. Wiersma, Reflection and Transmission of Waves near the Localization Threshold, Phys. Rev. Lett. **84**, 4333 (2000).

[32] N. Cherroret and S. E. Skipetrov, Microscopic derivation of self-consistent equations of Anderson localization in a disordered medium of finite size, Phys. Rev. E **77**, 046608 (2008).

[33] C. Tian, Supersymmetric field theory of local light diffusion in semi-infinite media, Phys. Rev. B **77**, 064205 (2008).

[34] C.-S. Tian, S.-K. Cheung, and Z.-Q. Zhang, Local Diffusion Theory for Localized Waves in Open Media, Phys. Rev. Lett. **105**, 263905 (2010).

[35] C. Tian, Hydrodynamic and field-theoretic approaches to light localization in open media, Physica (Amsterdam) **49E**, 124 (2013).

[36] D. Vollhardt and P. Wölfle, Diagrammatic, self-consistent treatment of the Anderson localization problem in $d \leq 2$ dimensions, Phys. Rev. B **22**, 4666 (1980).

[37] D. Vollhardt and P. Wölfle, Self-consistent theory of Anderson localization, in *Electronic Phase Transitions* (Elsevier Science, Amsterdam, 1992), p. 1.

[38] See Supplemental Material at http://link.aps.org/supplemental/10.1103/PhysRevLett.123.233903 for the justification of interpolation formulas for $D(z)$ in a slab, a full equation for $\langle I(z)\rangle_{\mathrm{SC}}$ at a mobility edge, a description of calculations performed for light scattering by cold atoms in a strong magnetic field, and a discussion of the role of two-atom subradiant states, which includes Refs. [39–43].

[39] P. Wölfle and D. Vollhardt, Self-consistent theory of Anderson localization: General formalism and applications, Int. J. Mod. Phys. B **24**, 1526 (2010).

[40] A. Fofanov, A. S. Kuraptsev, I. M. Sokolov, and M. D. Havey, Spatial distribution of optically induced atomic excitation in a dense and cold atomic ensemble, Phys. Rev. A **87**, 063839 (2013).

[41] S. E. Skipetrov, I. M. Sokolov, and M. D. Havey, Control of light trapping in a large atomic system by a static magnetic field, Phys. Rev. A **94**, 013825 (2016).

[42] S. E. Skipetrov and I. M. Sokolov, Transport of light through a dense ensemble of cold atoms in a static electric field, Phys. Rev. A **100**, 013821 (2019).

[43] F. Cottier, A. Cipris, R. Bachelard, and R. Kaiser, Microscopic and Macroscopic Signatures of 3D Anderson Localization of Light, Phys. Rev. Lett. **123**, 083401 (2019).

[44] Definitions of ξ in SC and SUSY models differ by a factor of 2.

[45] F. Evers and A. D. Mirlin, Anderson transitions, Rev. Mod. Phys. **80**, 1355 (2008).

[46] A. Rodriguez, L. J. Vasquez, and R. A. Römer, Multifractal Analysis with the Probability Density Function at the Three-Dimensional Anderson Transition, Phys. Rev. Lett. **102**, 106406 (2009).

[47] S. E. Skipetrov and I. M. Sokolov, Magnetic-Field-Driven Localization of Light in a Cold-Atom Gas, Phys. Rev. Lett. **114**, 053902 (2015).

[48] S. E. Skipetrov, Localization Transition for Light Scattering by Cold Atoms in an External Magnetic Field, Phys. Rev. Lett. **121**, 093601 (2018).

[49] L. D. Turner, K. F. E. M. Domen, and R. E. Scholten, Diffraction-contrast imaging of cold atoms, Phys. Rev. A **72**, 031403(R) (2005).

[50] D. V. Sheludko, S. C. Bell, R. Anderson, C. S. Hofmann, E. J. D. Vredenbregt, and R. E. Scholten, State-selective imaging of cold atoms, Phys. Rev. A **77**, 033401 (2008).

[51] A. A. Karabutov, I. M. Pelivanov, N. B. Podymova, and S. E. Skipetrov, Direct measurement of the spatial distribution of light intensity in a scattering medium, JETP Lett. **70**, 183 (1999).